

# DIFFUSION MODEL-BASED DATA AUGMENTATION FOR ENHANCED NEURON SEGMENTATION

Liuyun Jiang<sup>1,2</sup>, Yanchao Zhang<sup>1,2</sup>, Jinyue Guo<sup>1,3</sup>, Yizhuo Lu<sup>1,2</sup>, Ruining Zhou<sup>1,2</sup>, and Hua Han<sup>1,2\*</sup>

<sup>1</sup>State Key Laboratory of Brain Cognition and Brain-inspired Intelligence Technology, Institute of Automation, Chinese Academy of Sciences

<sup>2</sup>School of Future Technology, University of Chinese Academy of Sciences

<sup>3</sup>School of Artificial Intelligence, University of Chinese Academy of Sciences

## ABSTRACT

Neuron segmentation in electron microscopy (EM) aims to reconstruct the complete neuronal connectome; however, current deep learning-based methods are limited by their reliance on large-scale training data and extensive, time-consuming manual annotations. Traditional methods augment the training set through geometric and photometric transformations; however, the generated samples remain highly correlated with the original images and lack structural diversity. To address this limitation, we propose a diffusion-based data augmentation framework capable of generating diverse and structurally plausible image-label pairs for neuron segmentation. Specifically, the framework employs a resolution-aware conditional diffusion model with multi-scale conditioning and EM resolution priors to enable voxel-level image synthesis from 3D masks. It further incorporates a biology-guided mask remodeling module that produces augmented masks with enhanced structural realism. Together, these components effectively enrich the training set and improve segmentation performance. On the AC3 and AC4 datasets under low-annotation regimes, our method improves the ARAND metric by 32.1% and 30.7%, respectively, when combined with two different post-processing methods. Our code is available at <https://github.com/HeadLiuYun/NeuroDiff>.

**Index Terms**— electron microscopy, conditional diffusion models, data augmentation, neuron segmentation.

## 1. INTRODUCTION

Neuron segmentation aims to elucidate brain function by mapping neural connectivity and analyzing inter-neuronal signaling pathways. Advances in volume EM have enabled nanoscale reconstruction of three-dimensional neuronal structures [1, 2]; however, the increasing data scale and resolution pose significant challenges for automated processing. Deep learning-based segmentation methods rely heavily on large annotated datasets, making training both time-consuming and labor-intensive, while limited data diversity often results in overfitting and poor generalization.

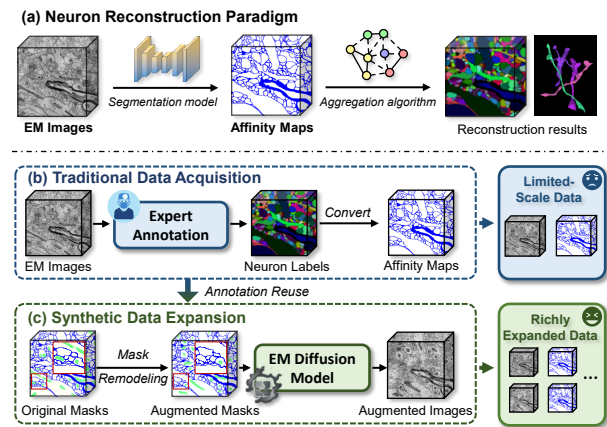


**Fig. 1.** (a) Illustration of the neuron reconstruction paradigm: EM images are processed by a segmentation network to generate affinity maps, which are aggregated by a post-processing algorithm to obtain the final reconstruction. (b) Traditional data acquisition relies on manual annotation for limited-scale training data. (c) Our method generates new image-label pairs to enrich the training dataset.

Data augmentation is a widely used technique to increase both the quantity and diversity of labeled data. Previous neuron segmentation methods [3] mainly rely on basic geometric and photometric transformations (e.g., flipping, rotation, brightness adjustment), which provide limited diversity and produce augmented images similar to the originals. Recently, generative model-based augmentation strategies have shown promising results in biomedical imaging [4, 5, 6], yet they have not been extended to 3D neuron segmentation in EM images. A key challenge lies in the precise voxel-level control required for the elongated, slender morphology of neurons.

To address the scarcity of training data and the challenges of neuron instance segmentation, as illustrated in Fig. 1, we propose a diffusion-based data augmentation framework for EM images. It improves segmentation performance by generating diverse and structurally plausible image-label pairs that enrich the training set. The framework comprises two key modules: a 3D EM image synthesis module and a 3D

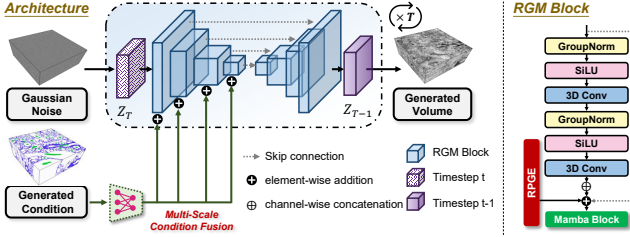


**Fig. 2.** Architecture of the proposed Resolution-Aware Conditional Diffusion model.

mask remodeling module. The synthesis module employs a conditional diffusion model to generate EM images from 3D masks, while the remodeling module produces augmented masks guided by boundary morphology, biological priors, and structural plausibility. By integrating both modules, our method synthesizes additional image-label pairs from existing data, effectively expanding the training set and enhancing segmentation performance.

The contributions of this work are summarized as follows: (1) We propose a diffusion-based data augmentation framework for neuron segmentation. (2) We integrate EM resolution priors into the diffusion model and incorporate biological priors and structural constraints into 3D mask remodeling to generate structurally consistent synthetic data. (3) Experimental results show that our method improves neuron segmentation performance and achieves state-of-the-art results, particularly under limited labeled data conditions.

## 2. METHOD

### 2.1. Resolution-Aware Conditional Diffusion

In this study, we employ a Denoising Diffusion Probabilistic Model (DDPM) [7] for 3D EM image synthesis. Following previous 3D diffusion studies [8, 5], we extend the U-Net to a 3D architecture for volumetric generation. In the forward process, Gaussian noise  $\epsilon \sim \mathcal{N}(0, I)$  is gradually added to the data  $x_0$  over  $T$  timesteps, where  $\beta_t$  represents the variance of the added noise:

$$q(x_{1:T} | x_0) = \prod_{t=1}^T \mathcal{N}\left(x_t; \sqrt{1 - \beta_t} x_{t-1}, \beta_t I\right) \quad (1)$$

In the reverse process, the model denoises the data from  $x_T$  to reconstruct  $x_0$ . For conditional generation, the U-Net takes both the noisy input  $x_T$  and the condition  $c$ , where  $c$  integrates mitochondrial masks and neuronal boundaries, since mitochondrial membranes affect the identification of neuronal boundaries. The conditional reverse diffusion process is defined as:

$$p_\theta(x_{t-1} | x_t, c) = \mathcal{N}(x_{t-1}; \mu_\theta(x_t, t, c), \Sigma_\theta(x_t, t, c)) \quad (2)$$

The U-Net predicts the mean  $\mu_\theta$  and variance  $\Sigma_\theta$ , while estimating the noise  $\epsilon_\theta$  to reverse the diffusion process. New

EM data  $x_0$  are generated by iteratively sampling  $x_{t-1} \sim p_\theta(x_{t-1} | x_t, c)$  for  $t = T, \dots, 1$ .

To enable voxel-level control, our denoising network incorporates two essential modules: the Multi-Scale Conditioning (MSC) module and the Resolution-Prior Guided Global Modeling (RGM) module.

**Multi-Scale Conditioning Module.** Different U-Net layers capture distinct semantic levels, and integrating conditions across multiple scales provides finer control. Therefore, we employ a multi-scale conditioning strategy rather than directly concatenating the condition  $c$  with  $x_T$ . Moreover, neuronal and organelle structures in EM images exhibit considerable variations in both size and morphology. The proposed multi-scale conditioning mechanism enables the model to synthesize large-scale structures while preserving fine details.

Let the input condition be  $c \in \mathbb{R}^{2 \times D \times H \times W}$ , where  $D$ ,  $H$ , and  $W$  represent the spatial dimensions of depth, height, and width. We first project  $c$  through several 3D convolutional layers to obtain a low-resolution, high-channel embedding  $c_{\text{embed}} \in \mathbb{R}^{256 \times D \times \frac{H}{8} \times \frac{W}{8}}$ . For each U-Net feature layer  $f_i \in \mathbb{R}^{C_i \times D_i \times H_i \times W_i}$ , the embedded feature  $c_{\text{embed}}$  is resized and processed by a zero-initialized convolution to produce  $c_i \in \mathbb{R}^{C_i \times D_i \times H_i \times W_i}$ . The aligned conditional feature is subsequently injected into the corresponding U-Net layer via element-wise addition:  $f_i \leftarrow f_i + c_i$ , as illustrated in Fig. 2.

**Resolution-Prior Guided Global Modeling.** Structures in EM images exhibit spatial continuity and connectivity, requiring the denoising network to capture global voxel dependencies for structurally consistent 3D generation. Mamba [9], a backbone built upon state-space models (SSMs) [10], offers linear computational complexity and excels in long-sequence modeling. Inspired by this property, we integrate Mamba into our denoising network to enable efficient and globally coherent 3D EM image synthesis.

Both Mamba and Transformers operate on serialized one-dimensional sequences. Vision Transformers [11] partition images into fixed-size patches and flatten them into vectors, which overlook intra-patch voxel relationships and constrain voxel-level tasks such as neuron segmentation. Leveraging Mamba's linear complexity, we directly flatten the 3D volume into a one-dimensional sequence to capture voxel-level dependencies without patch partitioning. To preserve 3D spatial context, we introduce a Resolution-Prior Guided Encoding (RPGE) module that incorporates the anisotropic resolution priors of EM images:

$$\text{RPGE}(z_i, y_i, x_i) = \text{MLP}([z_i \cdot r_z, y_i \cdot r_{xy}, x_i \cdot r_{xy}]) \quad (3)$$

where  $r_z$  and  $r_{xy}$  represent the axial and lateral resolutions of the EM volume, and  $(z_i, y_i, x_i)$  denote the coordinates of the  $i$ -th voxel. As illustrated in Fig. 2, the RPGE output is added element-wise within the RGM module and subsequently fed into the Mamba block for global modeling.

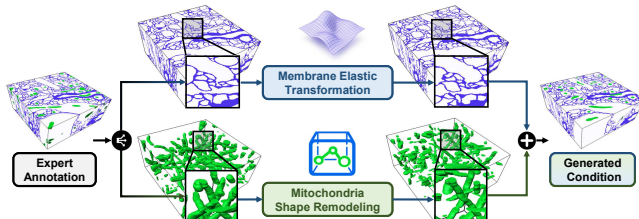


**Fig. 3.** Illustration of the Biology-Guided Mask Remodeling.

## 2.2. Biology-Guided Mask Remodeling

We observed that mitochondrial membranes can influence the identification of neuronal boundaries. Therefore, both neuronal boundaries and mitochondrial membranes are incorporated as conditional inputs, enabling the diffusion model to more effectively distinguish membrane types and generate EM images with higher fidelity, as shown in Fig. 3.

We first construct a mitochondrial signature library by extracting boundary-based morphological descriptors from existing mitochondrial masks. For each mitochondrion, boundary contour points are extracted, and an equivalent ellipse is fitted using second-order central moments to compute its major axis length and orientation. Subsequently, we propose a selective elastic deformation strategy for neuronal membrane enhancement. Specifically, elastic deformation is applied to the binary membrane mask (0–1) and utilized as a conditional input for EM image synthesis. Unlike previous approaches that deform the entire image, our method perturbs only membrane structures. Experiments demonstrate that selective membrane deformation yields notable improvements in neuron segmentation, likely because local perturbations introduce realistic boundary variations while preserving global structural integrity.

Next, mitochondria are placed on the binary mask of the elastically deformed neuronal membrane. Since mitochondria typically appear in larger neuronal cross-sections, the top 10% of neurons by volume are selected as candidate regions. Candidate neurons are randomly sampled, and ellipses are fitted to estimate their major axis lengths and orientations. Mitochondria from the signature library are then selected based on a predefined axis-length ratio relative to the corresponding neurons. During placement, each mitochondrion is aligned with the corresponding neuron's orientation, followed by morphological refinement and boundary validation to ensure a biologically plausible distribution. This process generates a new mask from the original, which can then be used to synthesize new EM images.

### 3. EXPERIMENTS

### 3.1. Datasets and Metrics

We used the AC3 and AC4 datasets from the mouse somatosensory cortex [12], imaged using scanning electron microscopy (SEM) at a resolution of  $6 \times 6 \times 29 \text{ nm}^3$ , with

**Table 1.** Comparison of segmentation performance using different synthesis methods for data augmentation across varying annotation ratios on the AC3/AC4 datasets. “Real images” refer to training with manually annotated data only.

Annotate(%)	Methods	Waterz		Multicut	
		VI ↓	ARAND ↓	VI ↓	ARAND ↓
4%	Real images	1.623	0.209	1.437	0.189
	Pix2Pix	1.779	0.222	1.461	0.141
	Med-DDPM	1.493	0.170	1.421	0.206
	Ours	<b>1.376</b>	<b>0.142</b>	<b>1.277</b>	<b>0.131</b>
20%	Real images	1.150	0.117	1.186	0.133
	Pix2Pix	1.185	0.135	1.342	0.218
	Med-DDPM	1.147	0.122	1.195	0.133
	Ours	<b>1.115</b>	<b>0.115</b>	<b>1.114</b>	<b>0.118</b>
100%	Real images	1.105	0.118	<b>1.116</b>	0.111
	Pix2Pix	1.451	0.161	1.769	0.290
	Med-DDPM	1.106	0.106	1.148	0.107
	Ours	<b>1.102</b>	<b>0.105</b>	1.135	<b>0.105</b>

**Table 2.** Quantitative results of generated image quality.

Methods		3D-FID↓
Pix2Pix		9.314
Med-DDPM		7.010
Ours		<b>6.203</b>

volumes of  $256 \times 1024 \times 1024$  and  $100 \times 1024 \times 1024$ , respectively. In our experiments, we used the AC4 volume for training and the first 100 slices of AC3 for testing. To assess the effectiveness of the proposed data augmentation strategy, we trained and evaluated neuron segmentation performance using 4%, 20%, and 100% of the available labeled data. We evaluated our method from two perspectives: assessing the quality of generated images and quantifying improvements in segmentation performance. To evaluate image quality, we adopted the widely used Fréchet Inception Distance (FID), extended to a 3D variant referred to as 3D-FID. Specifically, we pretrained a segmentation network on the AC3/AC4 datasets to extract feature representations and compute the distributional distance between real and generated images in the feature space, yielding the 3D-FID score. We evaluated neuron segmentation performance in EM images using two widely adopted metrics: Variation of Information (VI) and Adapted Rand Error (ARAND). Lower values for both metrics indicate better segmentation quality.

### 3.2. Implementation Details

Our experiments were conducted in two stages. In the first stage, the generative model was trained to synthesize new training samples, and in the second stage, the generated data were used to augment the training of the neuron segmentation network. Pix2Pix [13] and Med-DDPM [5] were used as baseline models, with their architectures adapted to 3D. Our model and Med-DDPM were trained for 10,000 iterations with a learning rate of  $1 \times 10^{-5}$ , a batch size of 1, and

**Table 3.** Comparison of segmentation performance with and without data augmentation using different methods on the AC3/AC4 datasets.

Methods	Waterz		Multicut	
	VI ↓	ARAND ↓	VI ↓	ARAND ↓
Superhuman[3]	1.150	0.117	1.186	0.133
SwinUNETR[14]	2.653	0.454	2.186	0.487
SegMamba[15]	1.467	0.206	1.410	0.232
Superhuman + Ours	1.115	0.115	1.114	0.118
SwinUNETR + Ours	2.294	0.375	1.921	0.419
SegMamba + Ours	1.387	0.187	1.269	0.177

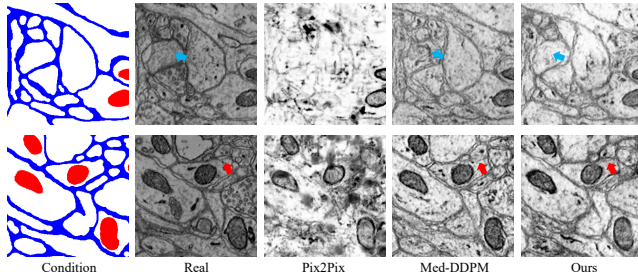


**Fig. 4.** Visualization of generated image quality. Blue arrows highlight potential artifacts, while red arrows indicate possible membrane loss.

input patch size of  $8 \times 512 \times 512$ . All subsequent neuron segmentation experiments employed the Superhuman [3] model, which was trained for 200,000 iterations with a learning rate of  $1 \times 10^{-4}$  and a batch size of 2. All models were trained on a single NVIDIA GeForce RTX 4090 GPU.

### 3.3. Comparison with State-of-the-art Methods

We compared the quality of images generated by different methods and evaluated the corresponding changes in segmentation performance after data augmentation. All segmentation models were trained from scratch and employed the same post-processing pipelines: Waterz [16] and Multicut [17]. For data augmentation using generated images, the ratio of augmented to original data was set to 1:1.

**Generated image quality.** We trained the generative model on 80 EM images of size  $512 \times 512$  from the AC4 dataset and generated samples for the remaining 20 slices. Table 2 reports the 3D-FID scores of the three methods, where our approach achieves the best performance. Fig. 4 shows EM images generated by different methods under conditional guidance. Benefiting from the MSC module, our method provides more precise structural control.

**Segmentation Results.** We conducted experiments on the AC3/AC4 datasets with three annotation ratios of 4%, 20%, and 100%. Table 1 compares the segmentation performance obtained using only annotated data and that obtained using both generated and annotated data. Our data augmentation method consistently achieves superior performance across all annotation ratios. Specifically, with a 4% annotation ra-

**Table 4.** Ablation of MSC and RGM.

MSC RGM	Waterz		Multicut		3D-FID↓
	VI ↓	ARAND ↓	VI ↓	ARAND ↓	
✓	1.765 1.649 1.587	0.180 0.164 0.162	1.577 1.565 1.425	0.174 0.172 0.140	6.838 6.734 6.603
✓	<b>1.376</b>	<b>0.142</b>	<b>1.277</b>	<b>0.131</b>	<b>6.203</b>

**Table 5.** Ablation Study on Mask Remodeling.

Methods	Waterz		Multicut	
	VI ↓	ARAND ↓	VI ↓	ARAND ↓
No Remodeling	1.427	0.156	1.331	0.138
Neuron-only	1.427	0.143	<b>1.252</b>	0.137
Mito-only	1.415	0.151	1.313	<b>0.131</b>
Ours	<b>1.376</b>	<b>0.142</b>	1.277	<b>0.131</b>

tion, our augmentation method improves the ARAND metric by **32.1%** and **30.7%** under two distinct post-processing settings. To further assess the generality of our method, we conducted experiments on three representative segmentation frameworks: the CNN-based Superhuman [3], the Transformer-based SwinUNETR [14], and the Mamba-based SegMamba [15]. As shown in Table 3, with a 20% annotation ratio, our data augmentation strategy consistently enhances the segmentation performance across all three models.

### 3.4. Ablation Studies and Analysis

We conducted ablation experiments using 4% of the labeled data to evaluate the effectiveness of the MSC and RGM modules. Table 4 summarizes the experimental results under different module configurations. In terms of both generated image quality and segmentation performance, the combined use of MSC and RGM achieves the best results. This finding suggests that generating more accurate neuronal imagery requires both multi-scale conditional guidance and global spatial connectivity modeling among voxels.

We further validate the effectiveness of Biology-Guided Mask Remodeling. Table 5 presents the experimental results for four settings: no remodeling, remodeling only the neuronal membrane, remodeling only the mitochondrial mask, and remodeling both simultaneously. The results indicate that jointly remodeling the neuronal membrane and mitochondrial mask produces more diverse training data, thereby achieving the best segmentation performance.

## 4. CONCLUSION

This paper proposes a diffusion-based data augmentation framework for neuron segmentation, which synthesizes new image-label pairs to enhance model training. Experiments demonstrate that our method effectively improves neuron segmentation performance.

## 5. COMPLIANCE WITH ETHICAL STANDARDS

This research study was conducted retrospectively using mouse subject data made available in open access [12]. Ethical approval was not required as confirmed by the license attached with the open access data.

## 6. ACKNOWLEDGEMENTS

This work was supported by the Beijing Natural Science Foundation (No. 5254042), the Brain Science and Brain-like Intelligence Technology – National Science and Technology Major Project (2022ZD0211900, 2022ZD0211902), and the National Natural Science Foundation of China (No. 32171461).

## 7. REFERENCES

- [1] Christopher J Peddie and Lucy M Collinson, “Exploring the third dimension: volume electron microscopy comes of age,” *Micron*, vol. 61, pp. 9–19, 2014.
- [2] Christopher J Peddie, Christel Genoud, Anna Kreshuk, Kimberly Meechan, Kristina D Micheva, Kedar Narayan, Constantin Pape, Robert G Parton, Nicole L Schieber, Yannick Schwab, et al., “Volume electron microscopy,” *Nature Reviews Methods Primers*, vol. 2, no. 1, pp. 51, 2022.
- [3] Kisuk Lee, Jonathan Zung, Peter Li, Viren Jain, and H Sebastian Seung, “Superhuman accuracy on the snemi3d connectomics challenge,” *arXiv preprint arXiv:1706.00120*, 2017.
- [4] Qi Chen, Mingxing Li, Jiacheng Li, Bo Hu, and Zhiwei Xiong, “Mask rearranging data augmentation for 3d mitochondria segmentation,” in *International Conference on Medical Image Computing and Computer-Assisted Intervention*. Springer, 2022, pp. 36–46.
- [5] Zolnamar Dorjsembe, Hsing-Kuo Pao, Sodtavilan Odonchimed, and Furen Xiao, “Conditional diffusion models for semantic 3d medical image synthesis,” *Authorea Preprints*, 2023.
- [6] Oleksandr Bailo, DongShik Ham, and Young Min Shin, “Red blood cell image generation for data augmentation using conditional generative adversarial networks,” in *Proceedings of the IEEE/CVF conference on computer vision and pattern recognition workshops*, 2019, pp. 0–0.
- [7] Jonathan Ho, Ajay Jain, and Pieter Abbeel, “Denoising diffusion probabilistic models,” *Advances in neural information processing systems*, vol. 33, pp. 6840–6851, 2020.
- [8] Zolnamar Dorjsembe, Sodtavilan Odonchimed, and Furen Xiao, “Three-dimensional medical image synthesis with denoising diffusion probabilistic models,” in *Medical imaging with deep learning*, 2022.
- [9] Albert Gu and Tri Dao, “Mamba: Linear-time sequence modeling with selective state spaces,” *arXiv preprint arXiv:2312.00752*, 2023.
- [10] Rudolph Emil Kalman, “A new approach to linear filtering and prediction problems,” 1960.
- [11] Alexey Dosovitskiy, Lucas Beyer, Alexander Kolesnikov, Dirk Weissenborn, Xiaohua Zhai, Thomas Unterthiner, Mostafa Dehghani, Matthias Minderer, Georg Heigold, Sylvain Gelly, et al., “An image is worth 16x16 words: Transformers for image recognition at scale,” *arXiv preprint arXiv:2010.11929*, 2020.
- [12] Narayanan Kasthuri, Kenneth Jeffrey Hayworth, Daniel Raimund Berger, Richard Lee Schalek, José Angel Conchello, Seymour Knowles-Barley, Dongil Lee, Amelio Vázquez-Reina, Verena Kaynig, Thouis Raymond Jones, et al., “Saturated reconstruction of a volume of neocortex,” *Cell*, vol. 162, no. 3, pp. 648–661, 2015.
- [13] Phillip Isola, Jun-Yan Zhu, Tinghui Zhou, and Alexei A Efros, “Image-to-image translation with conditional adversarial networks,” in *Proceedings of the IEEE conference on computer vision and pattern recognition*, 2017, pp. 1125–1134.
- [14] Ali Hatamizadeh, Vishwesh Nath, Yucheng Tang, Dong Yang, Holger R Roth, and Daguang Xu, “Swin unetr: Swin transformers for semantic segmentation of brain tumors in mri images,” in *International MICCAI brain lesion workshop*. Springer, 2021, pp. 272–284.
- [15] Zhaohu Xing, Tian Ye, Yijun Yang, Guang Liu, and Lei Zhu, “Segmamba: Long-range sequential modeling mamba for 3d medical image segmentation,” *arXiv preprint arXiv:2401.13560*, 2024.
- [16] Jan Funke, Fabian Tschopp, William Grisaitis, Arlo Sheridan, Chandan Singh, Stephan Saalfeld, and Srinivas C Turaga, “Large scale image segmentation with structured loss based deep learning for connectome reconstruction,” *IEEE transactions on pattern analysis and machine intelligence*, vol. 41, no. 7, pp. 1669–1680, 2018.
- [17] Thorsten Beier, Constantin Pape, Nasim Rahaman, Timo Prange, Stuart Berg, Davi D Bock, Albert Cardona, Graham W Knott, Stephen M Plaza, Louis K Scheffer, et al., “Multicut brings automated neurite segmentation closer to human performance,” *Nature methods*, vol. 14, no. 2, pp. 101–102, 2017.